

CrystEngComm

Accepted Manuscript



This is an *Accepted Manuscript*, which has been through the Royal Society of Chemistry peer review process and has been accepted for publication.

Accepted Manuscripts are published online shortly after acceptance, before technical editing, formatting and proof reading. Using this free service, authors can make their results available to the community, in citable form, before we publish the edited article. We will replace this *Accepted Manuscript* with the edited and formatted *Advance Article* as soon as it is available.

You can find more information about *Accepted Manuscripts* in the [Information for Authors](#).

Please note that technical editing may introduce minor changes to the text and/or graphics, which may alter content. The journal's standard [Terms & Conditions](#) and the [Ethical guidelines](#) still apply. In no event shall the Royal Society of Chemistry be held responsible for any errors or omissions in this *Accepted Manuscript* or any consequences arising from the use of any information it contains.

Low temperature solution processed ZnO/CuO heterojunction photocatalyst for visible light induced photo-degradation of organic pollutants

Shreyasi Pal^a, Soumen Maiti^a, Uday Narayan Maiti^b, and Kalyan Kumar Chattopadhyay^{a*}

^aThin Films and Nanoscience Laboratory, Department of Physics, Jadavpur University, Kolkata 700032, India, ^bKAIST, South Korea.

Corresponding Author: Email: kalyan_chattopadhyay@yahoo.com

Abstract:

Possibility of integrating manifold functionalities, coupled with various associated noble interface phenomena in the hierarchical nanoforms, either comprised of geometrical intricacies or achieved via rational coupling of several components, has made them immensely pertinent from both research and technological aspects. Here oxide based nanostructure hybrid has been realized by integrating low bandgap copper oxide nanosheet with high bandgap one dimensional zinc oxide nanowires on flexible carbon cloth as well as on flat substrate. This bandgap modulated hybrid nanostructures are generated for efficient absorption of visible light targeting their possible use in waste water management. Our work presents a novel ambient condition protocol for morphological tuning in the nanoscale or their organization in hierarchical structure. Environmental remediation through catalytic activity under visible light irradiation of the synthesized samples was inspected taking both anionic and cationic dyes (Methyl Orange and Rhodamine B respectively) as the model contaminants where the optimized heterostructure exhibits significantly better performance than mono component oxides. Such enhanced performance could be explained by the formation of favorable staggered gap multiple p-n

junctions at ZnO/CuO interface which in turns retard the photogenerated electron-hole pair recombination within the heterostructure. Signature of successful p-n junction formation at ZnO nanorod/CuO nanosheet interface has been identified via current–voltage measurement with a conducting tip AFM in contact mode. Creative designing of novel heterojunction adopting this protocol will pave the way for utilization of the entire visible range, thereby offering potential in solar energy conversion devices.

Introduction:

Driven by the urge to explore the manifold functionalities via combining the physical aspects of several materials, cutting edge research have garnered enormous worldwide interest regarding fabrication of novel heterostructures, where integration and direct interfacing of lower dimensional semiconductor frameworks into complex hierarchies is the well-trodden path.¹⁻⁸ Besides functional integration or rational designing of new materials, generation of improved or unusual features in these coupled systems has progressively advanced their auspicious adoption in multitudes of electronic and optoelectronic applications.⁹⁻¹² In such a scenario, focused research effort aiming at the creation of hetero-nanostructures having dual or multiple geometries with high mechanical robustness, optimum size and accurate chemical composition via suitable methodology is of paramount importance. Amongst metal oxide semiconductors, functionalized forms based on ZnO are widely recognized as the candidature of huge economic impact where the documented rich morphological assortment boost up their usage perspectives in applied fields such as UV detector,¹³⁻¹⁴ piezoelectric nano generator,¹⁵ solar cell^{16,17} etc. However, wide band gap of ZnO (~3.32 eV) impede the effective utilization of solar spectrum and they only absorb the ultraviolet irradiation (4% of the solar light) consequence of which poor photocatalytic

behavior was accounted. Additionally, as the functioning zone of pure ZnO based photocatalyst is only the UV region¹⁸⁻¹⁹ thus it suffers from widespread practical usage. Similar to ZnO, this narrow absorption spectral range factor associated with renowned photocatalyst, namely titanium dioxide (TiO₂) also confines their performances.²⁰ To broaden up this absorption range, pertinent development and exploration is highly desirable. For widening up the absorption range as well as to enhance the catalytic activity of these metal oxides, numerous protocols were adopted amongst which designing of morphology and facet tuned hierarchical architectures and coupling of one semiconductor with another semiconductor such as oxide or sulfide were the commonly accessed routes. Not restricted to the amalgamation of semiconducting nanostructures only, scientists have also attached several metals like Pt, Ag etc. with these metal oxides or doped them with suitable metals like La, Mn, Co etc. to achieve higher photodegradation performances.²¹⁻³⁰ Among the attached or decorated secondary material narrow band gap semiconductor is of great significance as they are economical and can overcome the aforesaid bottleneck. Copper oxide (CuO), a narrow band gap (~1.35 eV) p-type metal oxide has engendered extensive attention owing to their diversified applicability in electrochemistry,³¹ photo-conductivity,³² gas sensing³³ where the add-on features of non-toxicity and abundance availability of starting constituent (copper) lift up their potential insights. Despite the feasibility of high visible light absorption range the catalytic behaviour exhibited by pure CuO is surprisingly not appealing as it is largely restrained by high recombination rate of the photogenerated electron hole pair. Thus, to achieve high catalytic performance, a synergistic system may be visualized by coupling of ZnO and CuO where CuO acting as co-catalyst could extend the visible light response. Additionally, possible formation of favorable p-n junction at the nanostructure interface suppresses the photogenerated carrier recombination and thereby bestows improved performance. Hitherto,

documentations on this oxide based p-n hetero-contact were achieved mostly by electro-deposition, electro-chemical deposition or sputtering technique on flat substrate where the bottlenecks like small area growth, complex process control etc. associated with these protocol create some barriers over their universal application aspects.³⁴⁻³⁶ Furthermore, usage perspectives of this hybrid are mostly narrowed to sensing and photovoltaic application whereas their credential as visible light driven photocatalyst remains less cultivated till now.³⁷⁻⁴³ To explore the utility of ZnO/CuO hetero-junction over flexible substrate with their full potential, intriguing research effort focused towards facile as well as affordable and low thermal budgetary approach is of great significance from modest application point of views.

Here we present a simple and very convenient technique for large scale preparation of ZnO/CuO heterostructure, both on flexible and flat substrate just by dipping Cu coated ZnO substrate in chemical bath at complete ambient condition and via this approach, complexity regarding CuO synthesis over other metal oxide was eluded. Controlled tunability over heterostructure morphology was achieved by manipulating the metallic Cu coating over ZnO which in turn creates difference in junction formation at the interface. The photocatalytic activity was investigated by degradation of Methyl Orange (MO) and Rhodamine B (RhB) dye under visible light irradiation and a plausible enhancement mechanism for the superior photocatalytic activity based on p–n junction in the ZnO/CuO system was proposed. Moreover, registered current–voltage characteristic curve of the as-prepared heterojunction diode at room temperature with decent rectifying behaviour substantiated our hypothesis of formation of p-n hetero-contact at the interface of ZnO/CuO. Finally, such heterostructure as bi-functional materials with excellent electrical and catalytic properties may be envisaged as a potential candidate for diverse device applications like photovoltaic solar cells, sensors, electronic devices, photodetector and so forth.

Experimental:

Synthesis of ZnO nanorods:

Chemicals of analytic grade were used for synthesis of ZnO/CuO heterostructure. Firstly ZnO nanorod (NR) array was synthesized on flexible carbon cloth as well as on glass and ITO substrate by hexamine assisted simple wet chemical route as reported in our previous work. In brief, ZnO seed layer coated substrates were mounted on a glass slide and kept within 100 mL autoclavable Pyrex glass bottle containing equimolar aqueous solution of zinc nitrate ($\text{Zn}(\text{NO}_3)_2 \cdot 6\text{H}_2\text{O}$) and hexamine ($\text{C}_6\text{H}_{12}\text{N}_4$). The reaction was performed in a regular laboratory oven at 95 °C for 6 h. After the reaction span the bottle was allowed to cool down to room temperature and the substrate was washed with ample amount of deionized water (D.I.) water and dried in ambient air.

Synthesis of ZnO/CuO heterostructure:

Metallic copper (Cu) films with different thickness were deposited on the as synthesized ZnO NR via thermal evaporation where the coating thickness was carefully monitored by an in-situ microbalance of quartz crystal.

For the synthesis of ZnO/CuO heterostructure, firstly a solution was prepared by mixing each 10 mL of two separately prepared solutions of 0.038 M ammonium persulfate ($(\text{NH}_4)_2\text{S}_2\text{O}_8$) and 0.191 M sodium hydroxide (NaOH). Now, 2 mL of aforementioned mixture solution was added with 80 mL D.I. water and metallic Cu coated ZnO NR substrate was dipped for 6h at room temperature. Finally the substrate was washed with copious amount of D.I. water and dried overnight.

Additionally to understand the detail formation mechanism of the heterostructure, time-dependent experiments were also executed.

Characterization: Please see the supporting information†.

Photocatalytic Properties:

Photocatalytic activity of the products was examined with methyl orange (MO) (Aldrich) and Rhodamine B (RhB) dyes as the probe molecules under visible light irradiation (400W high-pressure mercury lamp (Philips) with a UV cut-off filter ($\lambda > 400$ nm)). Experimental procedures adopted to access the catalytic activity were: Samples (2×2cm) were vertically immersed in 40 mL aqueous solution of 10^{-5} M methyl orange/Rhodamine B and stirred for 60 min in complete darkness to attain adsorption/desorption equilibrium between the catalyst and dye. Thereafter it was irradiated with visible light where the distance between lamp to suspension surface was kept fixed at 15 cm. Small volumes of dye solution were withdrawn firstly after dark stirring and afterward in regular interval from the reactor and centrifuged. Finally, residual dye concentration in solution was quantified via monitoring the absorption intensity of dyes with SIMADZU UV-vis spectrophotometer.

Results & Discussion:

Low magnification FESEM image of ZnO NRs over flexible carbon fiber in Fig. 1a reveals large scale morphological uniformity over the substrate. Free standing ZnO NRs having the average

diameter and length ~ 250 nm and ~ 5 μm respectively were grown over the entire cylindrical surface of an individual fiber where the nanorods were radiating in outward direction from the axis of the fiber (Fig. 1a and its inset). Fig. 1 (d-l) illustrates three sorts of ZnO/CuO heterostructures over carbon cloth which manifests the impact of metallic Cu coating over ZnO nanorods in overall morphology determination. In all cases, high morphological uniformity of the synthesized products is obvious from the corresponding zoom out view in left panel of the Fig. 1. Sparse coverage and radial arrangement of CuO nanosheet over ZnO nanorod backbone is found to appear for nominal Cu coating (Fig. 1(d-f)). These sheets are ~ 500 nm in length and have a diameter that changes from ~ 50 to ~ 10 nm from the root to the tip. Relatively thicker and uniform Cu coating over ZnO NR leads to more complicated hierarchically intricate superstructures as huge number of sheet with higher dimensions appeared over the whole surface of the ZnO nanorod (Fig. 1(g-i)). Finally for very high metal coating, even bigger sized nanosheets not only gathered to form densely compact flower-like shape architecture formed on the top of ZnO NR also exhibited high superficial coverage (Fig. 1(j-l)). Additionally, for catalytic performance comparison of the heterostructures fabricated over flat and flexible substrate, this oxide-oxide hybrid was also realized over glass substrate, by adopting similar experimental protocol. Forest like morphology is highly noticeable from cross-sectional view in Fig. 1c where the main stems are ZnO nanorod and CuO sheets are branches. Finally, in the absence of underlying ZnO backbone, only CuO nanoflake evolved over carbon fiber (Fig. 1b) where very high coverage of them indicated the product homogeneity. Henceforth we will designate the heterostructure samples with nominal, moderate and high CuO coverage over ZnO as ZC-1, ZC-2 and ZC-3 respectively.

For precise investigation of the heterostructure morphology and the interconnection between two metal oxides (namely ZnO and CuO) TEM analysis were carried out. Underlying ZnO NRs with smooth side surfaces are evident from the TEM image (Supporting information Fig. S1(a)†). The average diameter of the ZnO NRs is observed to lie within a range of 100 to 150 nm. Well resolved lattice fringes running parallel to each other with assessed inter planar spacing of 0.26 nm corresponding to (002) plane of hexagonal wurtzite zinc oxide confirm the single crystal nature and [0001] as its preferred growth direction which could be unambiguously perceived from HRTEM image of a NR (Fig. 2a).⁴⁴ The single crystalline aspect is further ratified by the selected area diffraction pattern (SAED) containing well defined bright circular spot (Fig.2d). The entire ZnO NR surface, as could be seen from TEM image of ZC-2 (Fig. 2b), is homogeneously decorated by numerous CuO nanosheets which are tightly adhered to it. This randomly oriented, very thin sheets, having tip diameter ~15 nm, forms the outer shell and endorse the interface between two oxides. HRTEM investigation of an individual sheet reveals the crystalline nature of CuO as the estimated inter-fringe spacing of 0.25 nm is well consistent with the (111) crystal plane of monoclinic CuO (Fig.2h).⁴⁴ In addition, corresponding diffraction pattern taken from the sheet segment (Fig.2i) with circular ring signifies the polycrystalline nature of CuO. Further, TEM images of ZC-1 and ZC-3 in Fig. S1(b,c)† confirm the variances in CuO coverage over ZnO NRs and imitate the corresponding FESEM image. EDX spectrum of the ZC-2 sample taken from single carbon strand reveals that the heterostructure comprises of Zn, O, and Cu elements (Supporting information Fig.S2†) and corresponding elemental mapping in Fig. 2(c,e,g) shows their homogenous distribution. Based on the structural and compositional analysis of ZnO/CuO heterostructure, an atomic model is schemed and depicted in Fig. 2j, where the pink, green and yellow balls relate to Zn, O and Cu atom respectively. Further to demonstrate

the variance in CuO nanosheet coverage more explicitly, EDX analysis of the other two samples (ZC-1 and ZC-3) were also carried out and presented in supporting information (Fig. S2†). Comparison of the Cu/Zn atomic ratio in these samples suggests maximum ratio corresponds to ZC-3 and least for ZC-1 thereby highest CuO coverage for first one and nominal for the later.

Further, variance in CuO coverage over the underlying identical ZnO NR array also rendered changes in total surface area of these samples. Difference in surface area was confirmed from the Brunauer–Emmett–Teller (BET) surface area measurement via nitrogen (N₂) sorption. The corresponding N₂ adsorption–desorption isotherms of the heterostructure samples are presented in figure 3. The surface area of ZC-1, ZC-2 and ZC-3 samples is found to be 4.011 m²/g, 6.023 m²/g and 8.419 m²/g respectively. These results confirm maximum surface area for ZC-3 samples which is nearly 2 times higher than the ZC-1 sample and 10 times larger than that of carbon cloth (0.371 m²/g). The N₂ adsorption-desorption isotherms with such hysteresis loop at high relative pressure signify large surface area of the heterostructures. As the underlying ZnO NR substrate is identical in all heterostructures, these results clearly signify highest CuO coverage in ZC-3 sample as compare to others.

The crystal structure and phase purity of the ZnO/CuO heterostructure along with pristine ZnO were investigated via X-ray diffraction analysis (XRD) and the corresponding diffraction patterns are depicted in Fig. 4a. The star (*) marked peak present in all XRD profiles are associated with the underlying carbon cloth substrate which is conclusively verified by examining the XRD pattern of the bare substrate only (supporting information Fig. S3†). All remaining peaks in the diffraction pattern (I) and most number of the peaks in patterns (II, III and IV) display good congruity with those of the hexagonal wurtzite ZnO structure with lattice

constants of $a = 3.250 \text{ \AA}$ and $c = 5.206 \text{ \AA}$ (JCPDS card no. 36-1451). After CuO deposition, additional peaks appeared in XRD profiles which are related to ZC-1, ZC-2 and ZC-3 (II, III and IV) and can be indexed to monoclinic CuO with lattice constants of $a = 4.6853 \text{ \AA}$, $b = 3.4257 \text{ \AA}$, $c = 5.1303 \text{ \AA}$ (JCPDS card No. 80-1917). In absence of underlying ZnO, the XRD pattern of pure CuO nanoflake (supporting information Fig. S3†) matches well with monoclinic CuO. Finally nonappearance of any other impurity related peaks in the XRD profiles not only conclusively exclude the possibility of formation of any secondary phases but also highlight high purity of the samples.

To identify the chemical composition and oxidation state, XPS measurement of ZC-3 was carried out as the representative sample of these heterostructures. All the binding energies are calibrated by referencing the C 1s peak at 284.6 eV and corresponding results are shown in Fig. 4(b,c,d). XPS survey scan analysis reveals peaks corresponding to Zn, Cu, O and C where additional C related peak beyond the hetero-structural components results from carbon substrate as well as atmospheric carbon (supporting information Fig. S4†). High resolution XPS spectra corresponding to Zn 2p with intense doublet peaks centered at 1022.1 and 1045.1 eV point out +2 oxidation state of Zn. Moreover the assessed spin orbit splitting of 23 eV is commensurate well with existing literature.⁴⁵ The core level photoemission spectra corresponding to Cu 2p (Fig. 4b) shows peaks appearing at ~934 eV and ~954 eV which exhibit essentially identical binding energies of Cu 2p_{3/2} and Cu 2p_{1/2} respectively. Additionally, appearance of two shakeup satellite peaks on higher binding energy side indicates +2 oxidation state of Cu i.e. the formation of CuO.⁴⁶ Further, almost symmetric O1s spectra peaking at 530.7 eV corroborates well with the binding energy of O²⁻ ion in the metal oxide sites (i.e. ZnO, CuO).⁴⁷ These results validate the observed XRD investigation.

To further confirm the heterostructural composite formation, room temperature Raman analysis of ZC-3 and pristine ZnO samples were carried out and for simplistic comparison both were presented in same graph (Fig. 5). The spectrum corresponding to pristine ZnO NR is dominated by the presence of two strong peaks at ~ 436 and ~ 574 cm^{-1} which are arisen due to characteristic $E_2(\text{high})$ and $E_1(\text{LO})$ modes of ZnO respectively.⁴⁸ In comparison to the pristine ZnO NR, one strong additional peak at 286 cm^{-1} emerges in the ZC-3 spectrum which can be ascribed to A_{1g} mode of CuO originated due to the vibration of oxygen atoms.^{48,49} Further, the presence of Raman vibration modes related to ZnO and CuO together in same spectrum along with co-existence of these metal oxides in Raman spectral image (Fig. 5 inset: blue and green colour signify CuO and ZnO respectively) confirms the successful hetero-structure formation.

Time dependent morphological evolution:

For detail insight of the formation mechanism, a set of controlled experiments were carried out by varying the reaction time where the dimension of the underlying ZnO nanorods and thickness of the metallic Cu coating over nanorods were kept fixed. As a representative sample from the synthesized samples, we examined the temporal morphological evolution of ZC-3. From the FESEM image of Cu coated ZnO nanorods (Fig. 6a); formation of thick Cu film over the surface of ZnO is very much prominent. These films, comprising of numerous Cu nanoparticles, are responsible for making the nanorod seem visibly uneven, even though the surfaces of the coating particles are smooth. Only 10 min of reaction time were found to lead to the roughening of Cu coating surfaces as plentiful nano protrusions appeared from the surfaces which is obvious from Fig. 6b and its inset. Small extension in growth span (30 min) confers variance in the morphology in comparison to the priors, as not only the greater number of heightening notches

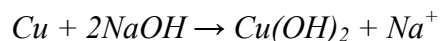
originated from the entire Cu surface, but also very few notches elevated abruptly to evolve into a sheet like shape (Fig. 6c and its inset). On further growth for a period of 60 min, these notches matured even more as all of them evolved into separate sheets (Fig. 6d with its inset) of which planar dimension of these sheets were measured to be ~250 nm. Such high coverage of CuO nanosheets generated a complex 3D hierarchical architecture, as a consequence of which the underlying ZnO nanorod became entirely invisible. Finally, the individual sheets with utmost dimension (300–500 nm in length) were finally obtained after 6 h of reaction time (Fig. 1(j-l)) which was designated as ZC-3.

Growth mechanism:

Based on aforesaid temporal evolution of CuO nanostructure, we propose a possible growth mechanism behind the formation of such heterostructures and it is shown schematically in Fig. 6e:

Firstly, the formation principle behind 1D growth of ZnO is governed by their intrinsic anisotropic crystal growth habit as a consequence of spontaneous polarization along C axis. At elevated temperature, hexamine decompose to OH⁻ ion and interacts readily with free zinc ion (Zn²⁺) in the solution, thus providing Zn(OH)₂ as intermediate, which in turn produce ZnO by dehydration.^{50,51} Detail formation mechanism of the ZnO nanorod was illustrated in our previous work.⁵⁰

Now, on immediate contact with high alkaline solution, smooth surfaces of metallic Cu over the ZnO nanorod becomes rough as the top surfaces of Cu turns to Cu(OH)₂ which serves as the nucleation site for further growth.⁴⁴ This dissolution reaction can be described as following:



Copper hydroxides, having layered brucite crystal structure preferentially grow in the form of 2D sheet i.e. along the layered plane.⁵² These hydroxide sheets, in strong oxidant environment (produce due to presence of ammonium persulphate) oxidizes and transforms to CuO where layered structure of copper hydroxide acts both as the precursor and the template.⁴⁴



As time progresses, continuous dissolution of the metallic Cu keeps providing the Cu(OH)₂ precursor for further growth of sheet like layered structures and this process continues until complete dissolution of the metallic core. Again due to strong binding interaction between the layered planes, these sheets tends to coalesce with each other and form sheets with bigger dimension which are manifested in the final product (ZC-3). Additionally, from the XRD profiles of time varied samples gradual increment of CuO to Cu ratio is very much prominent which substantiate the proposed growth hypothesis that CuO nanostructures evolved at the expense of metallic Cu (supporting information Fig. S5†).

Photocatalytic activity:

Out of the widespread applications of ZnO nanomaterials, their use for UV light induced eradication of organic dyes has become an area of recent scientific interest. On the other hand, CuO nanostructures also showed their potential as photocatalyst in the visible light region. Thus, by realizing heterostructures comprising of these oxides, we could expect enhancement in catalytic performance due to possible utilization of the total sunlight spectrum. Photocatalytic activity of the heterostructures along with detached singularities was measured with methyl

orange (MO) and Rhodamine B (RhB) dyes as the probe molecules under visible light irradiation. Prior to light exposure all the samples were treated in complete dark for 60 minutes to attain the adsorption/desorption equilibrium of the dye and samples. Evolution of UV-vis absorption spectra of MO at different irradiating time intervals as the result of photocatalytic activity of ZC-2 under visible light are presented in Fig. 7a. Gradual decrement of intensity of the characteristics absorption peak at 463 nm with increase of irradiation time was observed and after 280 minute it was found to decrease to 98%. For quantitative analysis of the photo-degradation behavior, decrease in dye content (C/C_0) as a function of time was plotted for ZC-1, ZC-2, ZC-3, ZnO and CuO samples (Fig. 7b), where C_0 and C signify the initial dye concentration after dark stirring ($t=0$) and final concentration (t) respectively. The dye content in the solution is proportional to the intensity of characteristics peak, therefore the ratio of C and C_0 is same to the absorption ratio at time $t=0$ and t . From the graph, highest degradation ability of ZC-2 sample as compare to others can be observed very prominently. Observed catalytic degradation experiment by visible light irradiation of MO follow the pseudo first order expression: $\ln(C_0/C) = k_{app}t$, where k_{app} is the apparent pseudo first order rate constant. Taking the slopes of the graphs of $\ln(C_0/C)$ versus irradiation time (t), (Fig. 7c), k_{app} value for all samples were estimated, which not only was found to be maximum for ZC-2, but also was found to be almost two times greater than the same for ZC-3. Further, for a facile comparative view, degradation percentages of all the photocatalysts after 40 min and 280 min. visible light irradiation are plotted in Fig. 7e. Gradual decoloration of MO as a consequence of the catalysis process can also be directly visualized from the digital image of dye solutions at different irradiation time interval where the initial deep orange color of MO monotonically decreases with increase of light exposure time (Fig. 7d). Instead of anionic methyl orange we also studied the

photo-degradation of another cationic dye namely Rhodamine B. With different dye, we observed the analogous catalytic result like methyl orange i.e. here also ZC-2 sample showed best photo-degradation ability among all (Fig. 8). For comparing performances, photocatalytic study using MO of the similar heterostructure (ZC-2) grown on glass was also carried out which interestingly exhibited inferior result than the same over fiber (supporting information Fig. S6†). Furthermore, materialization of the heterostructure over flexible carbon fabric provide additional boosts to the catalytic performances as it provides more extensive surface area than the flat glass substrate. Additionally, sufficient spacing between the individual units of the heterostructure as a consequence of due to woven like geometry of the underlying fiber promotes the mass transfer of dye. Similar sort of results for heterostructure on stainless steel mesh substrate was observed by Jung et al.⁵³

Due to the low coverage of CuO sheets over ZnO NR in ZC-1, inadequate amount of light absorption occurred and less number of photo-excited electrons-holes created; and consequently it shows weaker performance among the heterostructures. Again, from the BET measurement utmost surface area corresponds to ZC-3 is very obvious as compared to others. High surface area is always beneficial for photocatalysis as it increases the photocatalytic reaction centers for adsorption of reactant molecules. In this aspect ZC-3 should exhibit highest catalytic performance among all however very high superficial coverage of CuO nanosheets in ZC-3 may resist photogenerated carrier transference between stem ZnO NR and branch CuO thereby resulted in inferior catalytic performance than ZC-2.

Almost no decoloration of the hazardous dye in presence of ZnO alone under visible light could be attributed to the high band gap of ZnO which corresponds to UV region of the

electromagnetic radiation and offers very low absorption in the visible region. On the contrary, CuO nanoflake with high absorption in the visible region have the potential to be a good photocatalyst, but they demonstrate inferior performances as a consequence of their low band gap association due to which photo-generated electrons-holes recombination takes place very rapidly.³⁴ Additionally, poor catalytic performance exhibited solely by CuO nanoflake than heterostructures may also accounted from their relatively low surface area as compared to the later (clearly visible from FESEM image). Further, enhanced light absorption ability of the heterostructure as compared to pristine ZnO was confirmed by UV-vis analysis. The UV-vis diffuse reflectance spectra presented in supporting information (Fig. S7†) suggest very low reflection rate in the visible region thereby higher amount of light absorption by ZC-2 as compared to pristine ZnO.

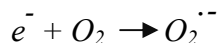
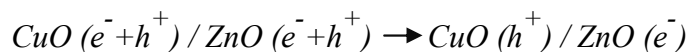
Further, pH dependent photocatalytic study of ZC-2 sample (supporting information S8†) suggests highest amount of MO degradation under acidic condition. Such result may accredit to the anionic configuration of MO as its adsorption is favored in acidic condition.⁵⁴ Similar sort of result was observed for another anionic dye namely AO7 by Jung et al.⁵³

To judge the figure of merit of the hybrid sample, catalytic efficiency of Degussa P-25 was also evaluated by degradation of methyl orange (MO) and compared with our best sample. (Supporting information Fig. S9†). Catalytic performance of Degussa P-25 was examined under visible light irradiation for 300 minutes. The dye degradation after 300 min is only ~12% for Degussa P-25 whereas the same for ZC-2 is ~98%. Such low photocatalytic performance illustrates the ineffectiveness Degussa P-25 in visible light and designate that methyl orange is partly induced by the band structure of Degussa P25 under visible light exposure.⁵⁵

To validate our hypothesis about p-n junction formation at CuO/ZnO hetero-structure interface, electrical measurement of sample fabricated on ITO substrate was carried out in air ambient at room temperature with a conducting tip AFM in contact mode. Schematic of the measurement set up along with typical asymmetric current–voltage (I-V) characteristics of the sample at appropriate bias voltage is presented in inset of Fig. 9a where bias voltage was applied across ITO and Au coated AFM tip. I-V characteristics with pronounced rectifying behavior and low turn on voltage ~ 1.87 V as well as low leakage current 0.95 nA at 3 V reverse voltage clearly portrays well-defined diode behavior of the heterostructure (Fig. 9a). Presentation of such nominal reverse leakage current by this heretojunction might be attributed to the low level of interface defect recombination between n-type ZnO and p-type CuO.⁵⁶ Furthermore, from semilog representation of the I-V characteristics (Fig. 9b), ideality factor of the diode was estimated using standard diode equation. The estimated ideality factor from the slope of the linear region of forward biased semilog I-V is curve was found to be 1.52 which is marginally greater than the ideal value of 1.02. Such results could be accredited to electrons and holes recombination in depletion region.⁵⁷ Finally, as compared to I-V characteristics of heterostructure the same for isolated one i.e. n-type ZnO NRs and p-type CuO nanoflakes separately (supporting information Fig. S10†) show good Ohmic behavior which corroborate our proposition that p-n junction only form when ZnO/CuO co-exist.

On the basis of above discussion, a photocatalytic reduction process of the dyes by ZnO/CuO heterostructure under visible light illumination is proposed and schematically shown in Fig. 10. Under visible light illumination, CuO gets excited and photogenerated electrons immigrate to CB of ZnO. These electrons, upon reacting with dissolved oxygen molecules form super-oxide

radical anion ($O_2^{\cdot-}$) which further indirectly turn into highly reactive hydroxide radicals (OH^{\cdot}). On the other hand, holes, by interacting with OH^- form highly reactive hydroxyl radicals. Reactive hydroxide radicals with high oxidation ability, generated though either photogenerated electrons or holes finally oxidizes the dyes. The total procedure can be formulated as follows:^{34,53}



Durability of the catalyst, an important criterion for their repetitive usage in environment remediation was next evaluated by photocatalytic degradation of MO for four cycles using the same film. ZC-2 sample exhibited remarkably high photo-stability even after four cycles as depicted in the photo-degradation plot in Fig. 11a. Under visible light exposure for 180 minute i.e. after first operation cycle, remaining MO concentration is only 2%. Small decline (<10%) in degradation efficiency was observed for ZC-2 sample where the residual concentration dye concentration after four operation cycles is only 10%. Such very small efficiency deterioration

suggests the high photo-durability and recyclability of the heterostructure. It is well known that high crystallinity of heterostructure renders the high photo-stability,⁴⁴ which is an analogue to our case where the high crystallinity is obvious from the TEM observations. Finally, FESEM image of ZC-2 in Fig. 11b after catalytic study shows no such differences with the previous which signifies high durability of the products.

Conclusions:

Decoration of solution processed ZnO nanowire with numerous CuO nanosheets was achieved via ambient condition synthesis protocol where extent of CuO growth was controlled in subtle fashion by deliberate manipulation of the metallic Cu coating over ZnO nanowire. Further, employing the same growth plan these heterostructures were realized both on flexible substrate as well as rigid one. Practical benefits of the heterostructures for photocatalytic applications were investigated under visible light where the heterostructures exhibited far better performance than the detached singularities and the catalytic activity of the heterostructures was varied with CuO coverage over ZnO. Manifested superior catalytic efficiency of heterostructure is hypothesized to be linked with quick and efficient photo-induced carrier separation originating from the favorable p-n junction formation at the interface and was validated by electrical measurement with a conducting tip AFM. Interestingly, heterostructure presented over flexible cloth substrate displayed greater result than the same over rigid substrate as the dense packing of the nanostructures hinders the mass transfer of dye. Heterostructure induced such catalytic performance enrichment under visible-light will direct researchers towards designing of novel photocatalyst materials comprising multifunctional oxides.

Acknowledgements:

SP wishes to thank the CSIR, the Council of Scientific and Industrial Research (CSIR), the Government of India., for awarding her a Junior Research Fellowship (JRF) during the execution of the work. The authors also wish to thank the University Grants Commission (UGC) for financial support under the ‘University with Potential for Excellence (UPEII)’ scheme.

Figure captions:

Fig. 1: Low magnification FESEM image of ZnO (a), CuO (b) coated carbon fabrics and ZnO/CuO heterostructure over glass substrate (c), insets show corresponding magnified views; FESEM image of three different heterostructures in different magnification ZC-1 (d-f), ZC-2 (g-i) and ZC-3 (j-l).

Fig. 2: HRTEM image (a) and SAED pattern (d) of ZnO nanorod; TEM images of ZC-2 with moderate magnification (b) and high magnification (f); HRTEM image (h) and SAED pattern (i) of CuO sheet; Elemental mapping of ZC-2 over a single carbon strand (c,e,g) and schematic atomic model (j).

Fig. 3: N₂ adsorption –desorption isotherms of the samples; (a) Carbon cloth, (b) ZC-1, (c) ZC-2 and (d) ZC-3.

Fig. 4: XRD patterns of the synthesized products (a); the XPS spectrum of Cu 2p (b) O1s (c) and Zn 2p (d) of ZC-3.

Fig. 5: Raman spectra of pristine ZnO and ZC-3, inset shows corresponding Raman spectral image of the heterostructure: blue and green color signify CuO and ZnO respectively.

Fig. 6: Morphological evolution of ZC-3 with time of (a) only coating (b) after 10 min, (c) 30 min and (d) 60 min. Insets exhibit the corresponding higher magnification images; (e) Schematic of the proposed growth mechanism.

Fig. 7: Temporal evolution of UV-vis absorption spectra corresponding to MO for ZC-2 (a); Decrease in the relative concentration of dye after different exposure times (b) and Kinetic plot of all samples (c); Digital images of dye solutions at different exposure times for ZC-2 (d) and degradation percentages of the samples after 40 and 280 min irradiation (e).

Fig. 8: Temporal evolution of UV-vis absorption spectra corresponding to Rhodamine B for ZC-2 (a); Decrease in the relative concentration of dye after different exposure times (b) and Kinetic plot of all samples (c); and digital images of dye solutions at different exposure times for ZC-2 (d).

Fig. 9: I–V characteristics of ZC-2 at room temperature (a) and its log–linear representation (b); Schematic of AFM I–V measurement (inset of a).

Fig. 10: Schematic of photocatalytic Mechanism of ZnO/CuO heterojunction.

Fig. 11: Relative dye concentration versus light exposure time for four consecutive cycles of operation for ZC-2 (a) FESSM image of ZC-2 sample after photocatalytic experiment (b).

Reference:

- (1) H. Kim, S. Jeon, M. Lee, J. Lee and K. Yong, *J. Mater. Chem.*, 2011, **21**, 13458.
- (2) R. R. Devarapalli, D. R. Shinde, F. Barka-Bouaifel, S. G. Yenchalwar, R. Boukherroub, M. A. More and M. V. Shelke, *J. Mater. Chem.*, 2012, **22**, 22922.

- (3) W. Tian, C. Zhang, T. Zhai, S.-L. Li, X. Wang, J. Liu, X. Jie, D. Liu, M. Liao, Y. Koide, D. Golberg and Y. Bando, *Adv. Mater.*, 2014, **26**, 3088.
- (4) S.-W. Choi, J. Y. Park and S. S. Kim, *Nanotechnology*, 2009, **20**, 465603.
- (5) N. D. Khoang, D. D. Trung, N. V. Duy, N. D. Hoa and N. V. Hieu, *Sens. Actuators, B*, 2012, **174**, 594.
- (6) D. R. Shinde, P. G. Chavan, S. Sen, D. S. Joag, M. A. More, S. C. Gadkari and S. K. Gupta, *ACS Appl. Mater. Interfaces*, 2011, **3**, 4730.
- (7) M. Lee and K. Yong, *Nanotechnology*, 2012, **23**, 194014.
- (8) Y.-C. Huang, S.-Y. Chang, C.-F. Lin and W. J. Tseng, *J. Mater. Chem.*, 2011, **21**, 14056.
- (9) D. Wu, Z. Gao, F. Xu, Z. Shi, W. Tao and K. Jiang, *CrystEngComm*, 2012, **14**, 7934.
- (10) U. N. Maiti, S. Maiti, T. P. Majumder and K. K. Chattopadhyay, *Nanotechnology*, 2011, **22**, 505703.
- (11) S. Maiti, U. N. Maiti, B. C. Behera, S. Pal and K. K. Chattopadhyay, *J. Mater. Chem. C*, 2013, **1**, 4940.
- (12) S. Warule, N. S. Chaudhari, B. B. Kale, K. R. Patil, P. M. Koinkar, M. A. More and R. Murakami, *J. Mater. Chem.*, 2012, **22**, 8887.
- (13) U. N. Maiti, K. K. Chattopadhyay, S. Karan and B. Mallik, *Scr. Mater.*, 2010, **62**, 305.
- (14) S. Maiti, U. N. Maiti, A. Chowdhury and K. K. Chattopadhyay, *CrystEngComm*, 2014, **16**, 1659.
- (15) Y. Qiu, H. Zhang, L. Hu, D. Yang, L. Wang, B. Wang, J. Ji, G. Liu, X. Liu, Ji. Lin, F. Li and S. Han, *Nanoscale*, 2012, **4**, 6568.

- (16) M.-L. Zhang, F. Jin, M.-L. Zheng, J. Liu, Z.-S. Zhao and X.-M. Duan, *RSC Adv.*, 2014, **4**, 10462.
- (17) H. Yan, Z. Yu, K. Lu, Y. Zhang and Z. Wei, *Small*, 2011, **7**, 3472.
- (18) R. Kumar, G. Kumar and A. Umar, *Mater. Lett.*, 2013, **97**, 100.
- (19) S. Ma, R. Li, C. Lv, W. Xu and X. Gou, *J. Hazard. Mater.*, 2011, **192**, 730.
- (20) J. Zhang, Q. Xu, Z. Feng, M. Li and C. Li, *Angew. Chem., Int. Ed.*, 2008, **47**, 1766.
- (21) C. Yu, G. Li, S. Kumar, K. Yang and R. Jin, *Adv. Mater.*, 2014, **26**, 892.
- (22) A. McLaren, T. V.-Solis, G. Li, and S. C. Tsang, *J. Am. Chem. Soc.*, 2009, **131**, 12540.
- (23) M. T. Uddin, Y. Nicolas, C. Olivier, T. Toupance, L. Servant, M. M. Müller, H.-J. Kleebe, J. Ziegler and W. Jaegermann, *Inorg. Chem.*, 2012, **51**, 7764.
- (24) L. Lin, Y. Yang, L. Men, X. Wang, D. He, Y. Chai, B. Zhao, S. Ghoshroy and Q. Tang, *Nanoscale*, 2013, **5**, 588.
- (25) C. Yu, K. Yang, Y. Xie, Q. Fan, J. C. Yu, Q. Shu and C. Wang, *Nanoscale*, 2013, **5**, 2142.
- (26) S. Anandan, A. Vinu, K.L.P. Sheeja Lovely, N. Gokulakrishnan, P. Srinivasu, T. Mori, V. Murugesan, V. Sivamurugan and K. Ariga, *J. Mol. Catal. A-Chem.*, 2007, **266**, 149.
- (27) Ruh Ullah and J. Dutta, *J. Hazard. Mater.*, 2008, **156**, 194.
- (28) Y. Lu, Y. Lin, D. Wang, L. Wang, T. Xie and T. Jiang, *Nano Res.*, 2011, **4**, 1144.
- (29) M. Basu, N. Garg and A. K. Ganguli, *J. Mater. Chem. A*, 2014, **2**, 7517.
- (30) S. Cho, J. -W. Jang, J. Kim, J. S. Lee, W. Choi and K. -H. Lee, *Langmuir*, 2011, **27**, 10243.
- (31) X. P. Gao, J. L. Bao, G. L. Pan, H. Y. Zhu, P. X. Huang, F. Wu and D. Y. Song, *J. Phys. Chem. B*, 2004, **108**, 5547.

- (32) S. Manna, K. Das and S. K. De, *ACS Appl. Mater. Interfaces*, 2010, **2**, 1536.
- (33) P. Raksa, A. Gardchareon, T. Chairuangstri, P. Mangkorntong, N. Mangkorntong and S. Choopun, *Ceram. Int.*, 2009, **35**, 649.
- (34) S. Wei, Y. Chen, Y. Ma and Z. Shao, *J. Mol. Catal. A: Chem.*, 2010, **331**, 112.
- (35) Q. Simon, D. Barreca, A. Gasparotto, C. Maccato, T. Montini, V. Gombac, P. Fornasiero, O. I. Lebedev, S. Turner and G. V. Tendeloo, *J. Mater. Chem.*, 2012, **22**, 11739.
- (36) K.-T. Liao, P. Shimpi and P. -X. Gao, *J. Mater. Chem.*, 2011, **21**, 9564.
- (37) M.-R. Yu, R.-J. Wu and M. Chavali, *Sens. Actuat. B-Chem.*, 2011, **153**, 321.
- (38) J. X. Wang, X. W. Sun, Y. Yang, K. K. A. Kyaw, X. Y. Huang, J. Z. Yin, J. Wei and H. V. Demir, *Nanotechnology*, 2011, **22**, 325704.
- (39) M.-R. Yu, G. Suyambrakasam, R.-J. Wu and M. Chavali, *Mater. Res. Bull.*, 2012, **47**, 1713.
- (40) M. H. Habibi, B. Karimi, M. Zendehtdel and M. Habibi, *Spectrochim. Acta, Part A*, 2013, **116**, 374.
- (41) H. Kidowaki, T. Oku and T. Akiyama, *J. Phys.: Conf. Ser.*, 2012, **352**, 012022.
- (42) M. H. Habibi, B. Karimi, M. Zendehtdel and M. J. Habibi, *Ind. Eng. Chem.*, 2014, **20**, 1462.
- (43) E. O. Omayio, P. M. Karimi, W. K. Njoroge and F. K. Mugwanga, *Int. J. Thin Film Sci. Tec.*, 2013, **2**, 25.
- (44) U. N. Maiti, S. Maiti and K. K. Chattopadhyay, *CrystEngComm*, 2012, **14**, 640.
- (45) U.N. Maiti, S. Maiti, S. Goswami, D. Sarkar and K. K. Chattopadhyay, *CrystEngComm*, 2011, **13**, 1976.
- (46) Z. Liu, H. Bai, S. Xu and D. D. Sun, *Int. J. Hydrogen Energ.*, 2011, **36**, 13473.

- (47) A. A. Ashkarran, A. I. zad, S. M. Mahdavi and M. M. Ahadian, *Appl. Phys. A*, 2010, **100**, 1097.
- (48) J. X. Wang, X. W. Sun, Y. Yang, K. K. A. Kyaw, X. Y. Huang, J. Z. Yin, J. Wei and H. V. Demir, *Nanotechnology*, 2011, **22**, 325704.
- (49) Y.-G. Lin, Y.-K. Hsu, S.-Y. Chen, L.-C. Chen and K.-H. Chen, *J. Mater. Chem.*, 2011, **21**, 324.
- (50) S. Maiti, U. N. Maiti and K. K. Chattopadhyay, *CrystEngComm*, 2012, **14**, 8244.
- (51) J. Qiu, X. Li, W. He, S. -J. Park, H. -K. Kim, Y. -H. Hwang, J.-H. Lee and Y. -D. Kim, *Nanotechnology*, 2009, **20**, 155603.
- (52) G. X. Pan, X. Xia, F. Cao, P.S. Tang and H. F. Chen, *Electrochim. Acta*, 2012, **63**, 335.
- (53) S. Jung and K. Yong, *Chem. Commun.*, 2011, **47**, 2643.
- (54) M. Shang, W. Wang and L. Zhang, *J. Hazard. Mater.*, 2009, **167**, 803.
- (55) D. Zhang, *Transition Met. Chem.*, 2010, **35**, 689.
- (56) I. Y. Y. Bu, *Ceram. Int.*, 2013, **39**, 8073.
- (57) Z. Ahmad and M. H. Sayyad, *Optoelectron. Adv. Mater., Rapid Commun.*, 2009, **3**, 509.

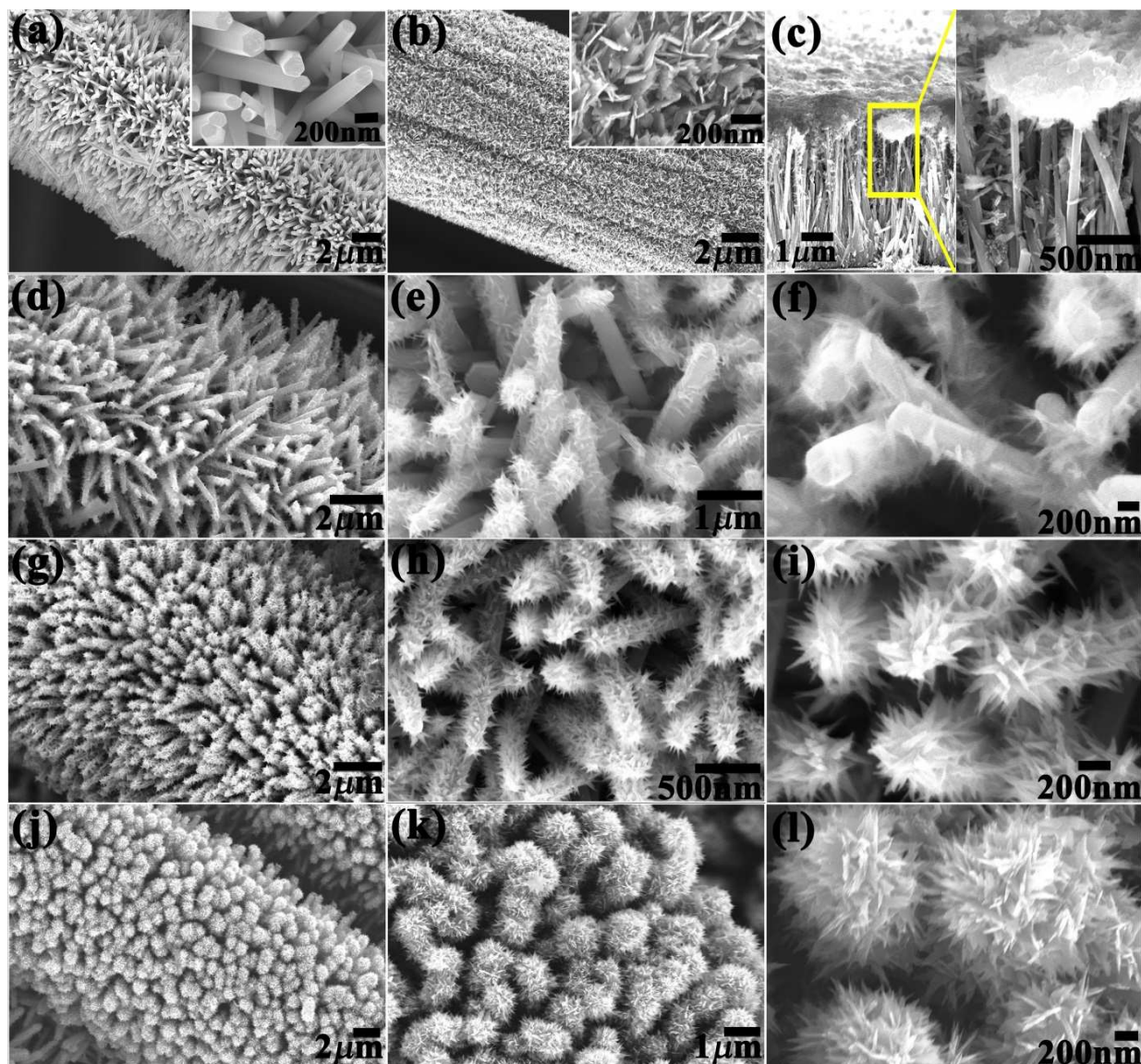


Fig.1: Pal et al.

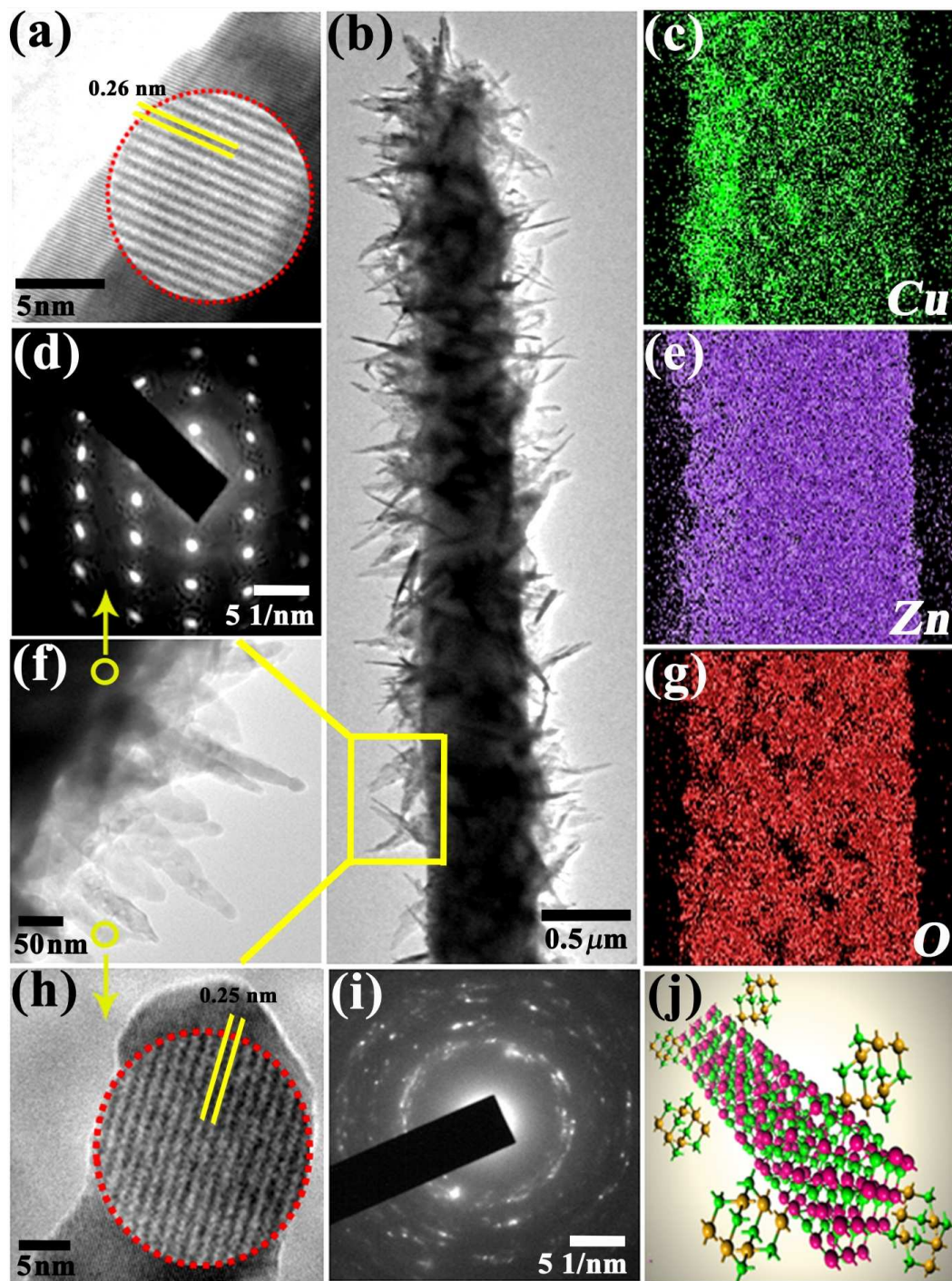


Fig.2: Pal et al.

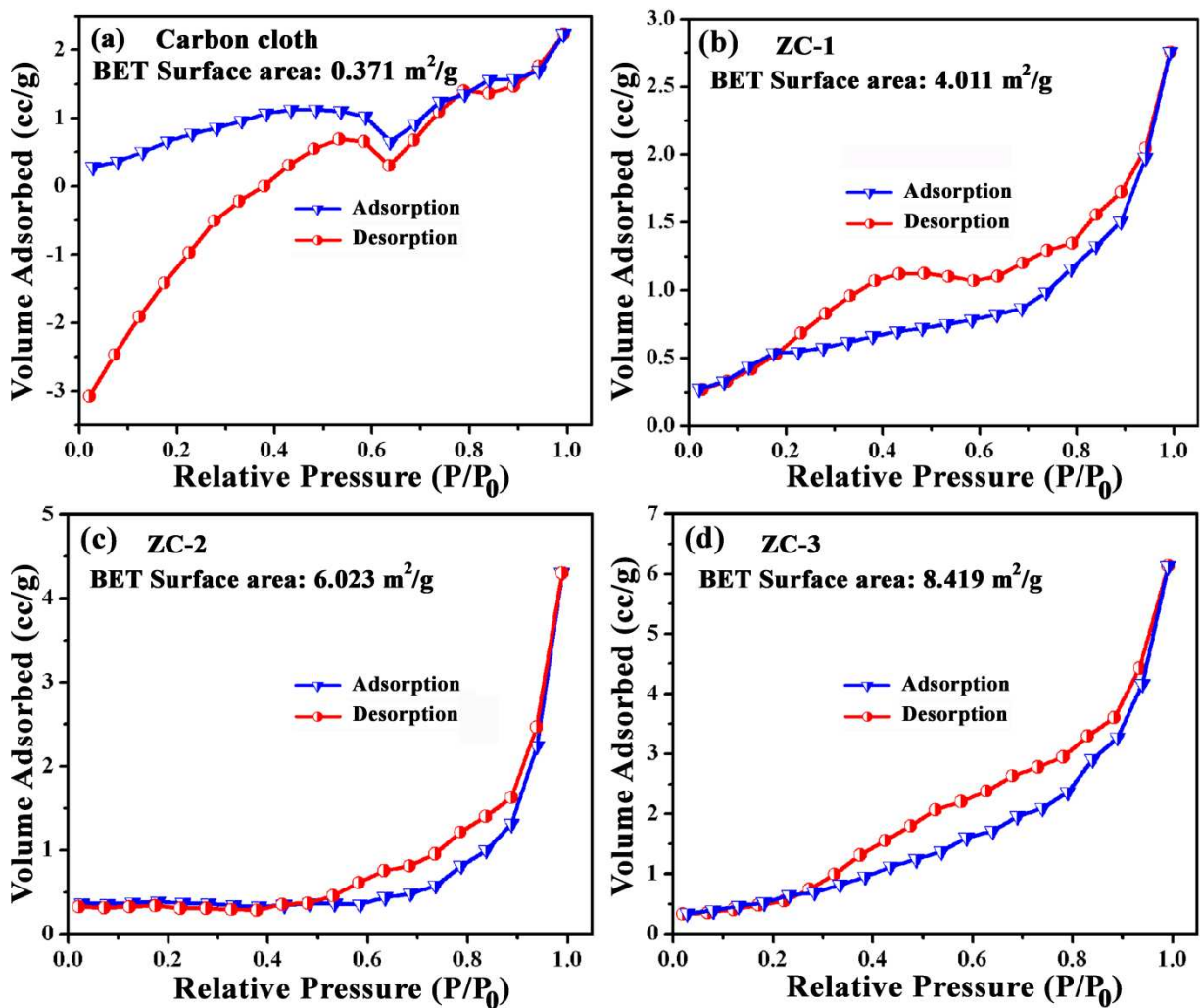


Fig.3: Pal et al.

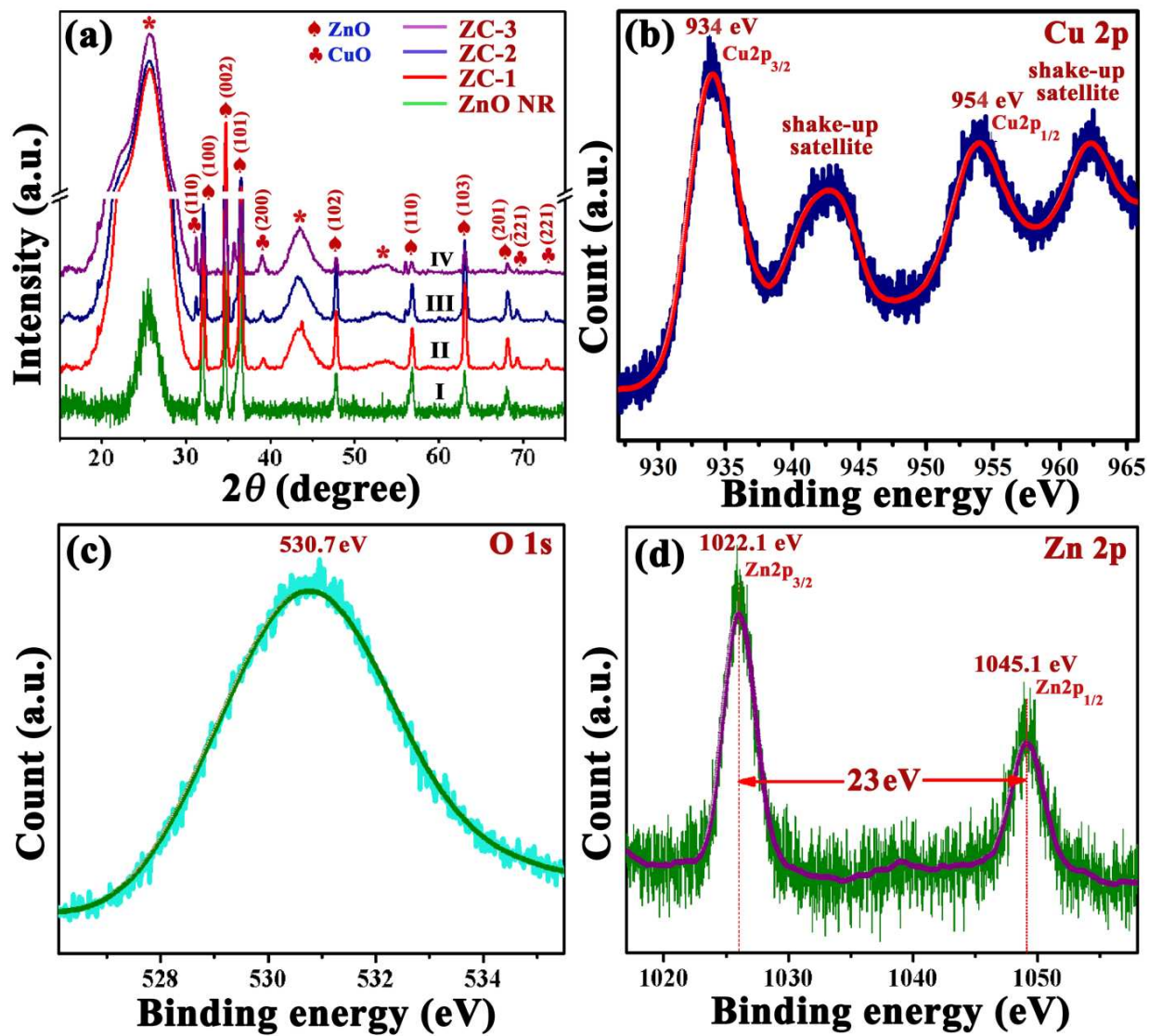


Fig.4: Pal et al.

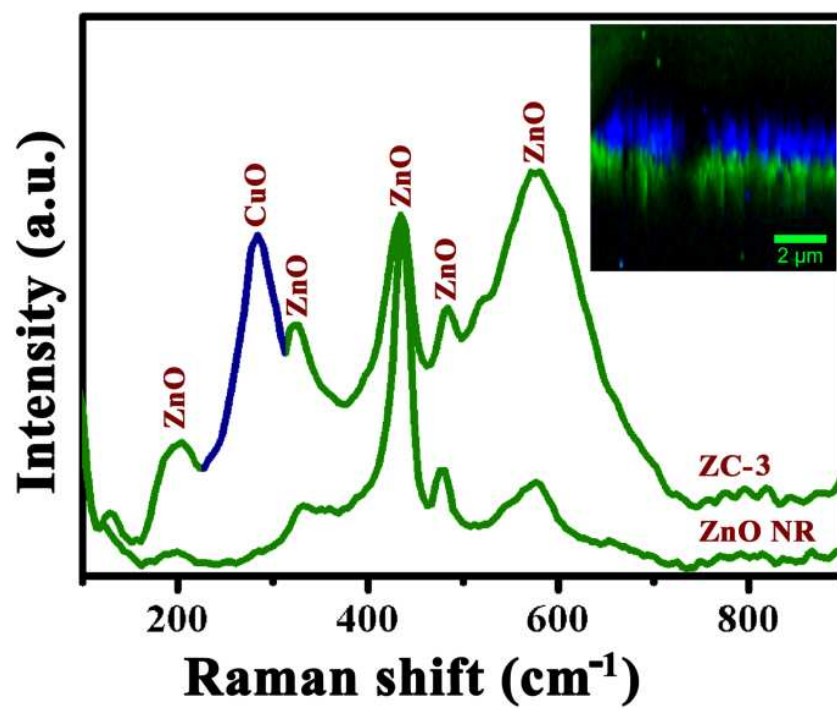


Fig.5: Pal et al.

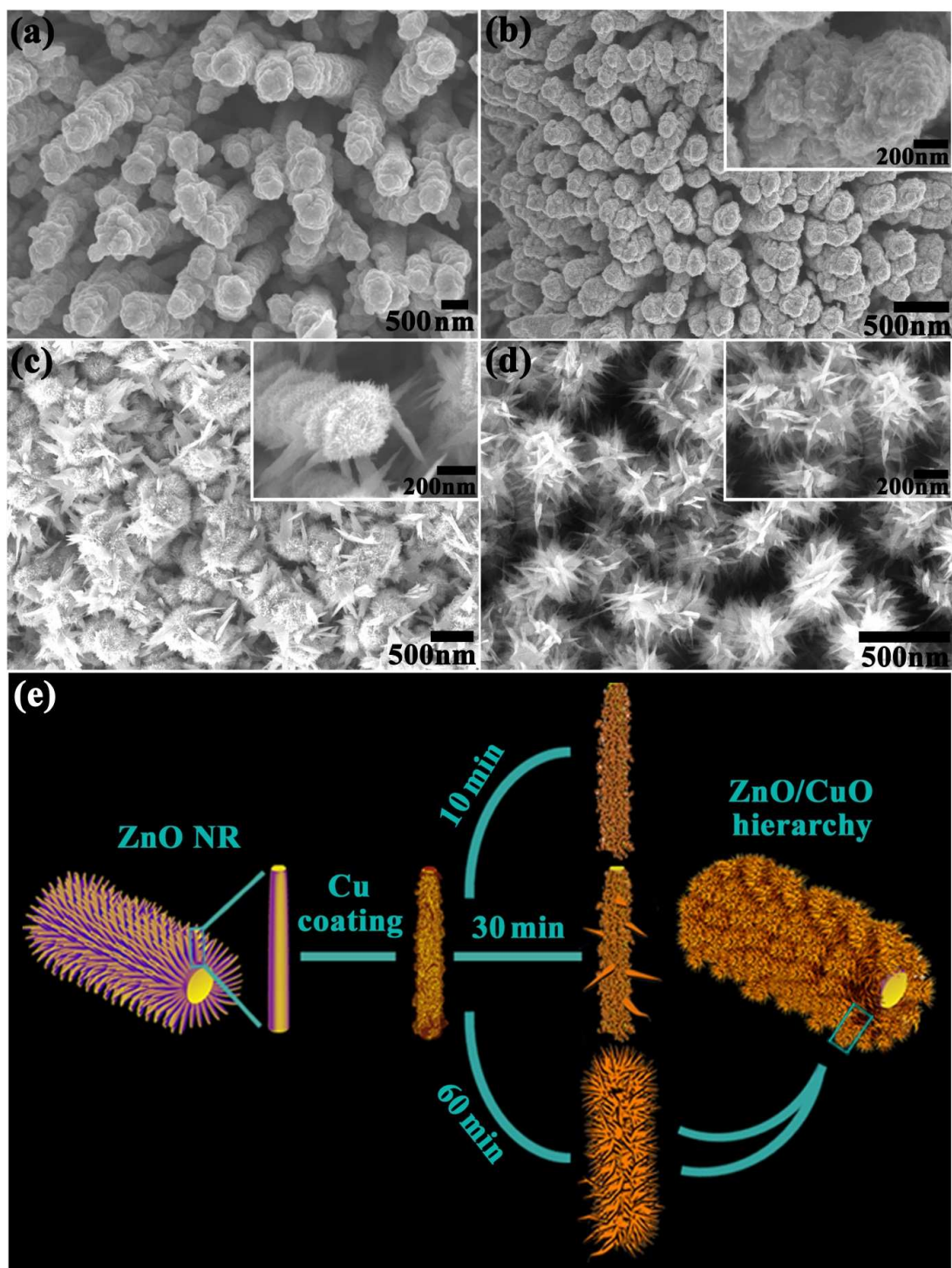


Fig.6: Pal et al.

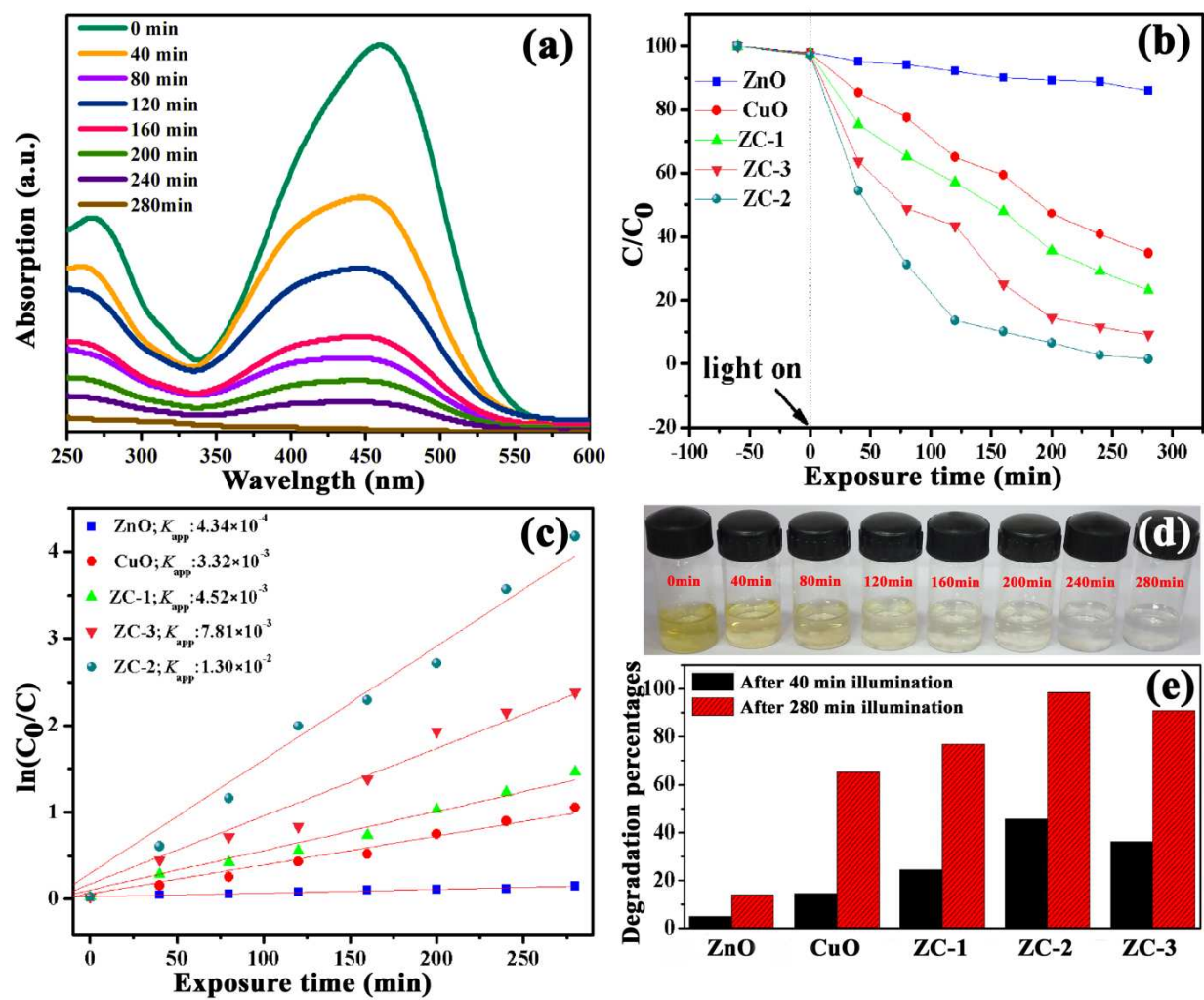


Fig.7: Pal et al.

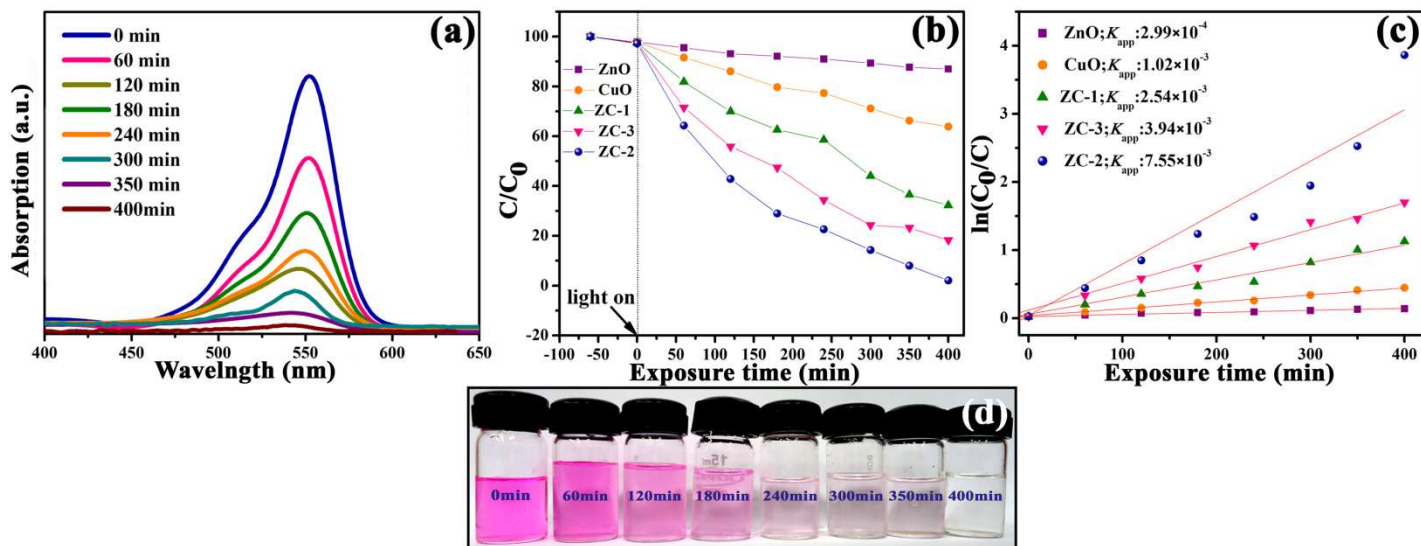


Fig.8: Pal et al.

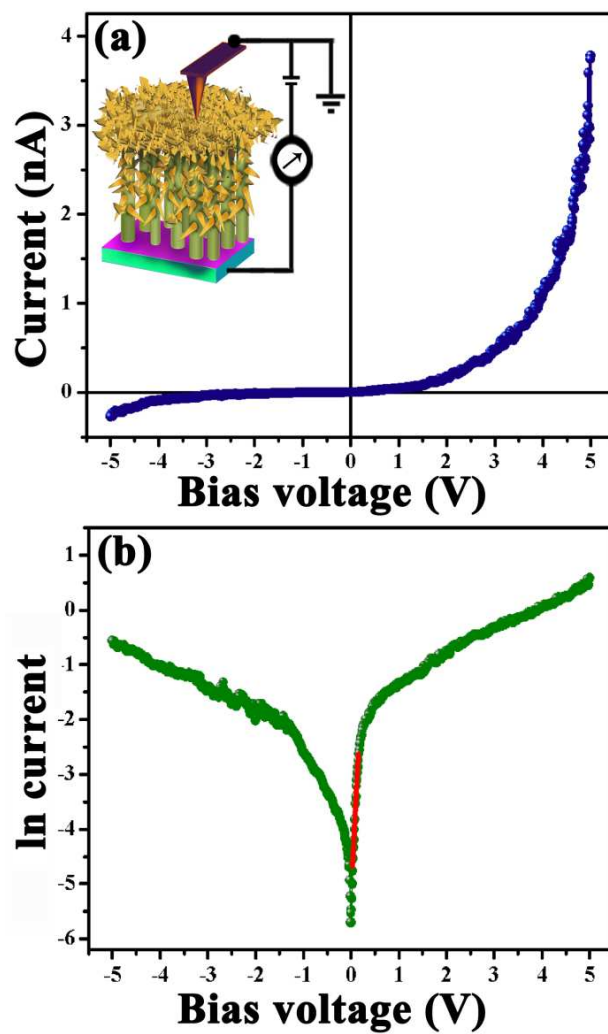


Fig.9: Pal et al.

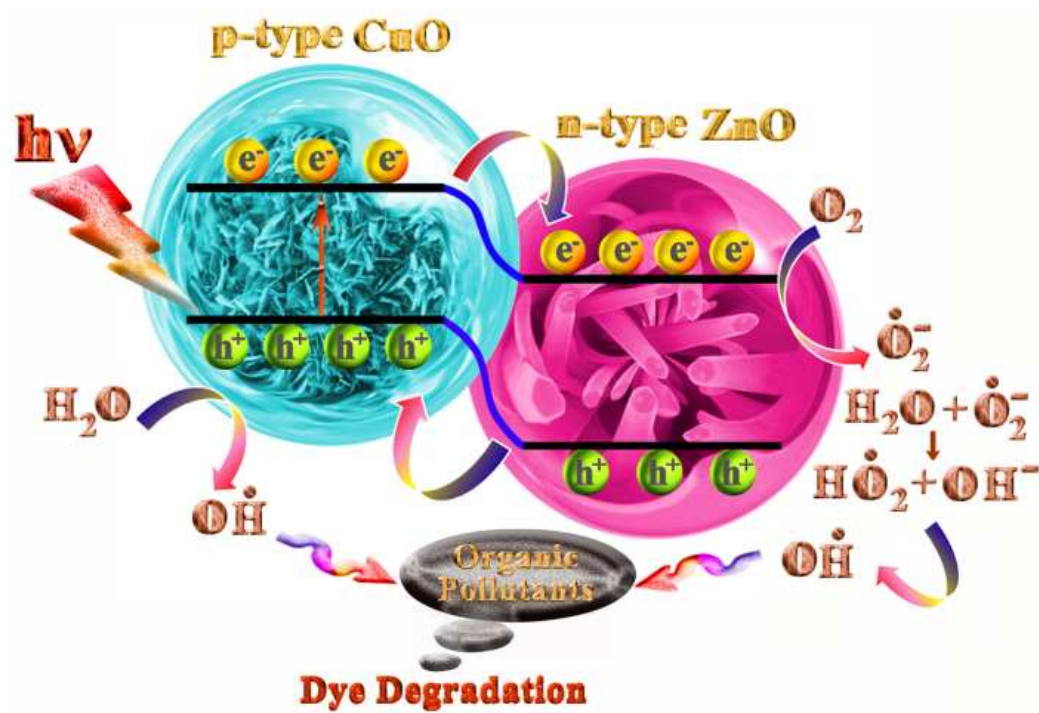


Fig.10: Pal et al.

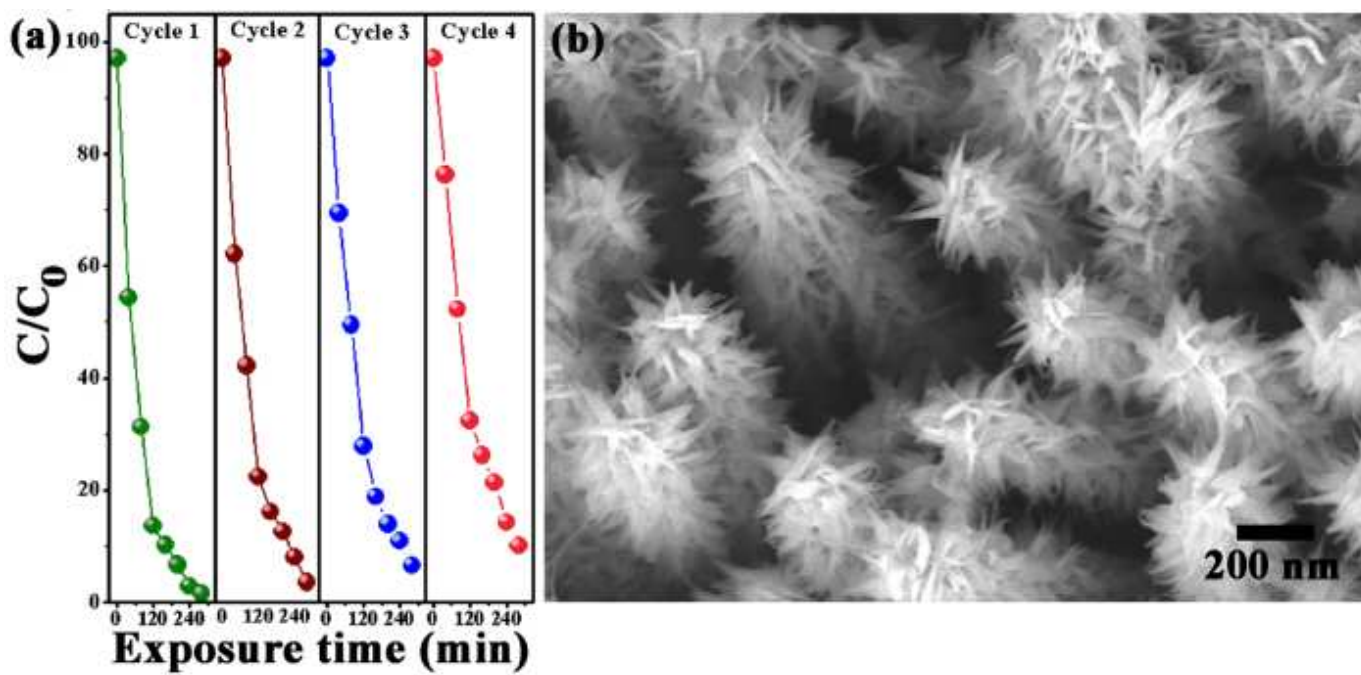


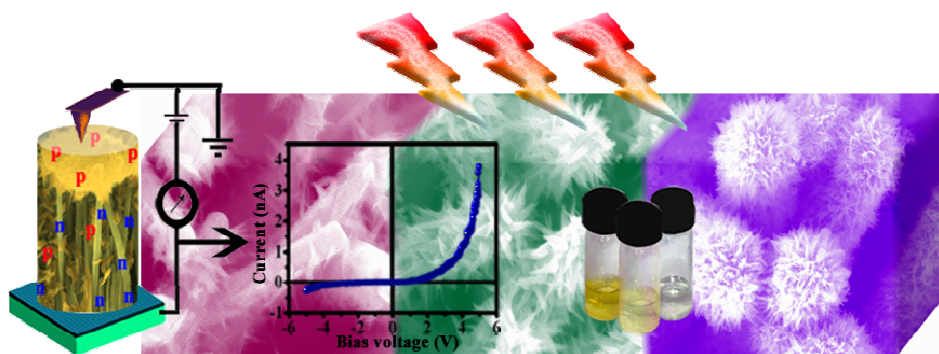
Fig.11: Pal et al.

Table of Content:**Low temperature solution processed ZnO/CuO heterojunction photocatalyst
for visible light induced photo-degradation of organic pollutants**

Shreyasi Pal^a, Soumen Maiti^a, Uday Narayan Maiti^b, and Kalyan Kumar Chattopadhyay^{a*}

^aThin Films and Nanoscience Laboratory, Department of Physics, Jadavpur University, Kolkata 700032, India, ^bKAIST, South Korea.

Corresponding Author email: kalyan_chattopadhyay@yahoo.com



Morphology controlled hierarchical ZnO/CuO architecture was realized on both flexible and rigid substrates exhibiting excellent photocatalytic performance by virtue of favourable heterojunction formation at nanostructure interfaces.